Elastic moduli and hardness of highly incompressible platinum perpnictide $PtAs_2$

Oliver Tschauner, Boris Kiefer, Florent Tetard, Kimberly Tait, Judith Bourguille, Andreas Zerr, Przemyslaw Dera, Alastair McDowell, Jason Knight, and Simon Clark

Citation: Appl. Phys. Lett. **103**, 101901 (2013); doi: 10.1063/1.4819143
View online: https://doi.org/10.1063/1.4819143
View Table of Contents: http://aip.scitation.org/toc/apl/103/10
Published by the American Institute of Physics

Elastic moduli and hardness of highly incompressible platinum perpnictide $PtAs_2$

Oliver Tschauner,[1] Boris Kiefer,[2] Florent Tetard,[3] Kimberly Tait,[4] Judith Bourguille,[3] Andreas Zerr,[3] Przemyslaw Dera,[5] Alastair McDowell,[6] Jason Knight,[6] and Simon Clark[6]
[1]*High Pressure Science and Engineering Center, Department of Geoscience, University of Nevada, Las Vegas, Nevada 89154, USA*
[2]*Department of Physics, University of New Mexico, Las Cruces, New Mexico 88003, USA*
[3]*LSPM-CNRS, 99 av. J. B. Clément, 93430 Villetaneuse, France*
[4]*Department of Earth Sciences, University of Toronto, 22 Russell St., Toronto, Ontario M5S 3B1, Canada*
[5]*Argonne National Laboratory, University of Chicago, 9700 S Cass Avenue, Argonne, Illinois 60439, USA*
[6]*Advanced Light Source, Lawrence Berkeley Laboratory, Berkeley, California 94720, USA*

(Received 24 June 2013; accepted 30 July 2013; published online 3 September 2013)

$PtAs_2$ appears to be the least compressible known arsenide with a bulk modulus of 220(5) GPa and a shear modulus of between 64 and 77 GPa. $PtAs_2$ has a hardness of 11(1) GPa, which is remarkably high for an arsenide. These elastic and mechanical properties in combination with the known chemical inertness and the small indirect band gap add interest to the use and occurrence of $PtAs_2$ at Pt-GaAs contacts in transistors. We note the modest fracture toughness of 1.1–1.6 MPa $m^{1/2}$ of $PtAs_2$. © *2013 AIP Publishing LLC*. [http://dx.doi.org/10.1063/1.4819143]

Perpnictides of the platinum group elements (PGEs) are semimetallic ($PtSb_2$, $PtBi_2$)[1,2] or semiconducting (PtP_2, $PtAs_2$)[2,3] isotypic compounds which assume the pyrite structure. $PtAs_2$ has found interest as—intentionally or inadvertently occurring—phase in transistors with Pt/GaAs interfaces where it generates limited degradation.[4,5] The discovery of the highly incompressible and potentially superhard PGE perpnictides PtN_2, IrN_2, OsN_2 (Refs. 6–10) raise the question of the mechanical properties of the PGE perpnictides with heavier pnictide anions. While the electronic properties of the heavy PGE perpnictides have been examined,[1–3] their mechanical properties have remained unknown. $PtAs_2$ as an intermediate phase in Pt-GaAs or Pt-AlAs contacts may affect the Schottky barrier heights if its shear elastic strength is markedly higher than that of Pt and GaAs or AlAs.

Here we present experimentally and computationally determined elastic moduli, nanoindentation- and Vickers hardness values for platinum perarsenide, $PtAs_2$ (sperrylite).[11] We show that $PtAs_2$ exhibits an unusually high bulk and shear modulus and an unusually high hardness for an arsenide. Its fracture resistance is low. We discuss possible origins of this unusual mechanical behavior and implication of $PtAs_2$-bearing contacts in transistors.

Natural single crystal specimens of $PtAs_2$ (Sperrylite) from the typolocality Vermillion Mine, Ontario, Canada were obtained from the Royal Ontario Museum. The crystals were idiomorphic pentagondodecahedra of 0.5–1.5 mm diameter and were examined with an SEM for chemical composition: Neither Bi or Sb or S nor other PGEs than Pt were detected beyond trace levels in this sample. Three sample crystals were embedded in random orientations in epoxy resin and polished for indentation measurements. One crystal was cleaved and a crystal piece of 100 μm edge length and 10 μm thickness was examined by XRD for crystal quality and then loaded in a symmetric diamond anvil cell with X-ray translucent c-BN backing plates and with neon as pressure transmitting medium. Pressure was measured by the redshift of the R1 Cr^{3+} fluorescence line of ruby using the scale established by Dewaele *et al.*[12]

Single crystal X-ray diffraction data as function of pressure were collected at beamline 12.2.2 ALS with 30.000(1) keV primary beam energy and a MAR345 image plate detector. Image plate frames were collected at φ angles between $-15°$ and $+15°$ and between 165° and 215° in 1° increments with $\pm 0.5°$ oscillation.

The GSE-ADA data collection package[13] was used for peak search and fitting, and for absorption correction. The RSV software[13] was used for indexing and cell refinement. Between 180 and 200 reflections were observed and fitted. In order to assess eventual strain-induced and spontaneous lattice deformation unit cell refinements were conducted both with cubic metrics—and without symmetry constraints. Above 35 GPa, the diffraction data indicate anisotropic strain both through peak shapes and unit cell deformation and were not used in the determination of the equation of state. The origin of this strain was not further examined here although the small $R_{int} < 0.08$ (Ref. 14) suggest that the strain is from non-hydrostatic stress rather than from a phase transition. Structure analysis was conducted using Shelxl (Ref. 14) for refining the x fractional coordinate of As and the U_{iso} of Pt and As with the final weighted refinement factor[14] R_1 between 0.08 and 0.10 using 14 to 20 unique reflections. Refined cell volumina, cell parameters, isotropic thermal displacement factors and the As x-fractional coordinates up to 35 GPa, 300 K are given in Table I.

Nanoindentation testing was performed in the continuous stiffness mode using an XP Nanoindentor (MTS, Oak Ridge, TN, USA) with a Berkovich indenter. Maximal penetration was 700 nm and maximal load 110 mN. A series of ten tests for each of three single crystal samples in random orientation was performed at a constant strain rate of $0.05\,s^{-1}$. Reduced elastic modulus, E_r, and nanohardness, H_n, were obtained by averaging the data for displacements between 400 and 600 nm. Combining the experimental K_0 and E_r values, we derived the shear modulus G_0 of $PtAs_2$ using the established

TABLE I. Cell volumina and fractional atomic coordinates of $PtAs_2$ at pressures between 0 and 35 GPa. The U_{iso} of Pt was found to be 0.010 ± 0.005 Å^2 and the U_{iso} of As was 0.018 ± 0.05 Å^3 throughout the pressure range.

Pressure (GPa)	Volume (Å^3)	x
0	212.46(5)	0.383(1)
0.86	211.9(1)	
2.90	209.8(1)	
3.96	208.57(6)	0.383(1)
6.20	206.00(6)	
8.89	204.33(7)	
11.24	201.41(9)	0.382(2)
14.14	198.5(1)	
19.00	195.12(8)	0.382(1)
23.01	191.18(6)	
27.65	187.15(9)	0.382(2)
34.61	183.1(5)	

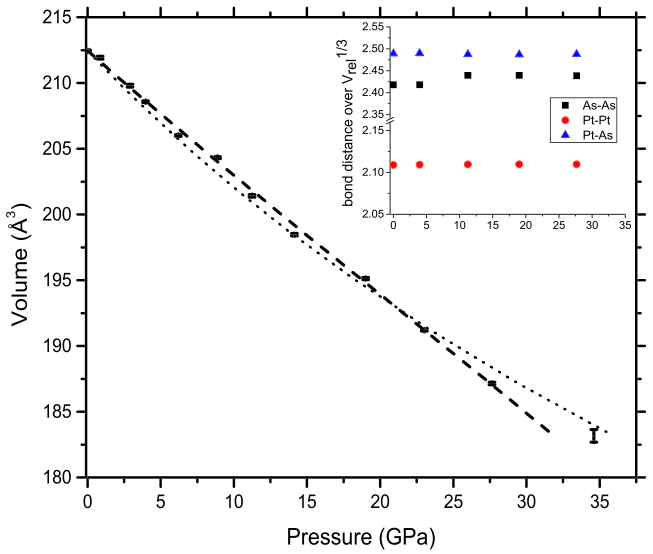

FIG. 1. Compression behavior of $PtAs_2$. The highest pressure data point was not included in the fitting of the equation of state because of indications for non-hydrostatic stresses acting on the sample. Compression of $PtAs_2$ is basically linear over at least 30 GPa. Dashed line: 3rd order Birch-Murnaghan fit with a K_0' of 1.1, dotted line: same but with K_0' fixed to 4. Obviously, the fit with $K_0' = 4$ mismatches the observed compression behavior. The inset shows the Pt-Pt, Pt-As, and As-As interatomic distances normalized by the cubic root of the relative volume $V_{rel} = V(P)/V_0$. Pressure induced changes in the structure are marginal.

procedure.[15] Indentations remaining on the sample surfaces as well as generated cracks were examined by atomic force microscope (AFM) in contact mode. Silicon tips with a force constant of 2.8 N/m and a nominal radius of curvature of 20 nm were employed. The crack lengths were used to estimate the fracture resistance, K_{Ic}, of $PtAs_2$.

The Vickers microhardness, H_V, was measured on flat, mirror quality polished surfaces of three crystals using a Duramin-X hardness tester (Struers, Denmark). Indentations (two measurements for each sample crystal and every load) were made by applying loads of 10, 25, 50, and 100 g. No higher loads were applied due to pervasive cracking. The load time was fixed to 15 s in each case. The impression diagonals and the crack lengths were measured using a SEM Zeiss Supra 40VP with 5 kV accelerating voltage providing a spatial resolution of about 2 nm.

Figure 1 shows the evolution of unit cell volume as function of pressure. Obviously the compression is close to linear over the pressure range of 0 to 30 GPa. At 35 GPa anisotropic strain was observed in the unit cell refinements and this data point was not included in the equation of state. There is no volume offset or change in compressibility observed upon crystallization of the neon pressure medium at ~4 GPa. We obtain a bulk modulus K_0 of 222 ± 3 GPa with a fixed K_0' of 0 and a K_0 of 217 ± 2 GPa with a K_0' of 0.41 ± 0.51 using a Vinet equation of state. Using a 3rd order Birch-Murnaghan equation of state, we obtain a K_0 of 216 ± 2 GPa with a K_0' of 1.1 ± 0.3. Because of the small pressure derivative of the bulk modulus, K_0', we consider the Vinet equation of state more appropriate than the Birch-Murnaghan equation which is biased towards K_0' values around 4.[16] In fact, a 3rd order Birch-Murnaghan equation of state with a fixed K_0' of 4 gives a K_0 of 180 GPa. However, as shown in Figure 1, this fit overestimates compression at low pressures and underestimates compression at high pressures, because the pressure-derivative of K_0 is clearly smaller than 4. We also note that K_0 raises to 266 ± 7 GPa when including the volume data collected at 35 and 42 GPa. However, these higher pressure data are probably affected by anisotropic stress (see above). Therefore, we disregard these data here and conclude that the K_0 of $PtAs_2$ is 220 ± 5 GPa and K_0' is between 0 and 1. The bulk modulus of 220 ± 5 GPa is unusually high for an arsenide. For instance, the bulk modulus of the structurally related $FeAs_2$ has been calculated to 154 GPa.[17] Monoarsenides such as LaAs and LuAs exhibit even lower K_0 of 92 and 85 GPa, respectively.[18] Even $B_{12}As_2$ has a slightly lower bulk modulus of 216 GPa.[19] Similarly, chalcogenides in the pyrite structure exhibit significantly lower bulk moduli of 133 GPa for pyrite FeS_2 (Ref. 20) and of 83 GPa for vaesite, NiS_2.[21]

We look at the evolution of structural parameters with pressure. In Figure 1 (inset) the Pt-Pt, Pt-As, and As-As interatomic distances are normalized by the cubic root of the volume (which equals the lattice parameter in this case) at each pressure and plotted versus measured pressure. Thus, changes in atomic positions that deviate from volume compression are visible by deviations from lines parallel to the pressure axis. As one can see from Figure 1 (inset), only the As-As interatomic distance (that is, the perarsenide bond) expands slightly with respect to bulk compression. However, the Pt-As distance evolves just along bulk compression. $PtAs_2$ is isotypic to pyrite. Hence, the Pt atoms reside on the nodes of an fcc lattice while the centers of the perarsenide units match the nodes of another fcc lattice shifted relative to the Pt lattice by $\frac{1}{2},\frac{1}{2},\frac{1}{2}$. Thus, compression shifts the non-bonding Pt d_{xy}, d_{yz}, and d_{xz}-orbitals of t_{2g} symmetry, that are oriented along the cubic axes, towards the As-As $pp\pi$ states (here we refer to the sterical configuration of orbitals in the PGE-persulfides[22] which can be expected to be similar in isotypic $PtAs_2$). No new bonds form over the examined pressure interval: Otherwise a structural change (if minor) would occur. Instead, compression increases the Coulomb repulsion which gives rise to the observed low compressibility. Of course, the same kind of bond configurations in the same crystal structure occur in vaesite NiS_2 with a bulk modulus of only 83 GPa (Ref. 21) and pyrite FeS_2 with a bulk

modulus of 133 GPa.[20] However, the 5*d* electrons of Pt are better screened from the nucleus than the 3*d* electrons in Fe and Ni. Hence, repulsion is expected to be higher for the high Z compound along directions of non-orthogonal states. Moreover, considering the general trend of electronegativity and following the calculations of Nguyen *et al.*[23] there is markedly more charge transfer between cations and anions in FeS_2 and NiS_2 as compared to $PtAs_2$. Thus, increasing pressure is expected to allow more charge transfer from Fe and Ni toward S and reduced Coulomb repulsion while in $PtAs_2$ the transfer is reverse (according to our calculations of Bader charges—see below) and repulsion enhanced with increasing compression. These effects cause the observed low compressibility of $PtAs_2$. Because of the very limited structural degrees of freedom and the high symmetry, it is expected that this compression mechanism remains valid as long as $PtAs_2$ remains in the pyrite structure. In fact, the internal structural coordinate are almost pressure invariant (Figure 1, inset). This explains the unusual low pressure-derivative of the bulk modulus.

Nano-indentation measurements gave a reduced modulus E_r between 177(2) and 201(4) GPa for three crystals in different orientation Using the correlation between reduced, bulk-, and shear elastic modulus of sample and indentor[15] the shear modulus G_0 of $PtAs_2$ was estimated to between 64(2) and 77(2) GPa.

Nanoindentation hardness, H_n, of $PtAs_2$ showed clearly the indentation size effect for all of the single crystal samples (Figure 2) as one observes a continuous decrease of H_n with increasing indentation load: For instance, for sample B we obtain $H_n \approx 19$ GPa at L = 2.5 mN (~0.25 g), $H_n \approx 17.2$ GPa at 40 mN (~4 g), and $H_n \approx 15.8$ GPa at 60 mN (~6 g). In both, the H_V—and the nanoindentation measurements the indentation size effect continues without discontinuity to higher loads and flattens out between 50 and 100 g (Figure 2). The microhardness of $PtAs_2$ at the highest loads, averaged over three samples, is found to be $H_V = 11(1)$ GPa.

In both H_n and H_V measurements, we observed formation of extended cracks indicating a high brittleness, and accordingly low fracture toughness, K_{Ic}, of $PtAs_2$. From the crack length, we estimated K_{Ic} using our measured elastic moduli and hardness data according to (Refs. 24 and 25). Assuming a "half-penny" crack configuration, we obtained for all three crystal samples a fracture toughness of $K_{Ic} = 1.1(3)$ MPa $m^{1/2}$. Assuming Palmqvist crack profiles and following the procedure described by Laugier,[26] the K_{Ic} value is somewhat higher (1.4–1.6 MPa $m^{1/2}$). A similar result ($K_{Ic} = 1.3 - 1.6$ MPa $m^{1/2}$) was obtained from the H_V indentations using the Shetty's equation.[27–30] However, the latter values have to be considered with caution because the high brittleness of the material leads to the formation of long and/or multiple cracks as well as to splitting of the material around the indentation. This behavior was especially pronounced for higher loads.

Comparison of the experimental H_V value with G_0 shows that $PtAs_2$ falls well within the range of the well established correlation of these two material properties (Figure 3). In particular, $PtAs_2$ compares to transition metal mononitrides and-carbides such as ZrN, NbC, etc. in terms of hardness and to GaP and cubic ZrO_2 in terms of the correlation of shear elastic stiffness and hardness.

We conducted first-principle computations using VASP[31,32] with local density approximation (LDA)[33] and general gradient approximation (GGA)[34] exchange-correlation functionals, with a planewave cutoff of 600 eV, and a Γ-centered 8 × 8 × 8 k-point mesh. Electron–ion interactions were treated within the all-electron like Projected Augmented Wave formalism.[35,36] The valence configuration (core-radii) were $[Xe]6s^1 5d^9$ ($R_{core} = 2.5\ a_B$) and $[Ar]4s^2 4p^3$ ($R_{core} = 2.1\ a_B$) for Pt, As for both LDA and GGA, respectively. The electronic structure was integrated using the Blochl tertrahedron method. Convergence with these settings was better than 1 meV/atom. The ground state of the $PtAs_2$ structure was determined by simultaneous relaxation of all degrees of freedom. Energy and pressure for the equation of

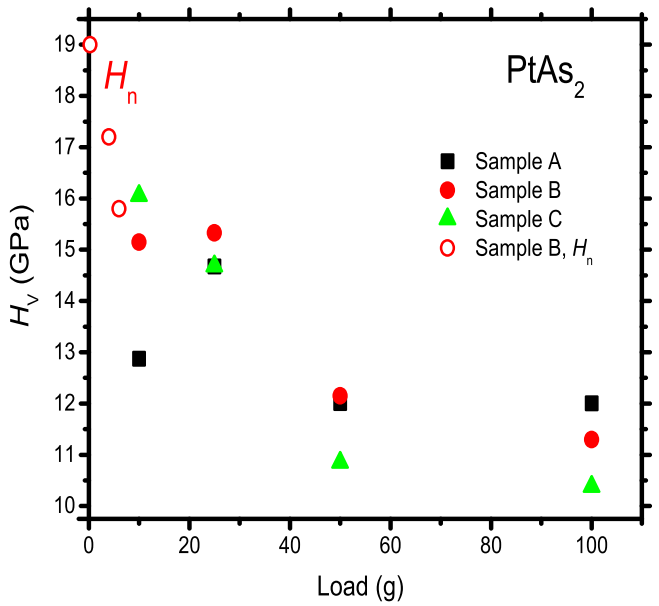

FIG. 2. Nanoindentation (open symbols, sample B) and Vickers microindentation (solid symbols, samples A, B, and C) data obtained in this work.

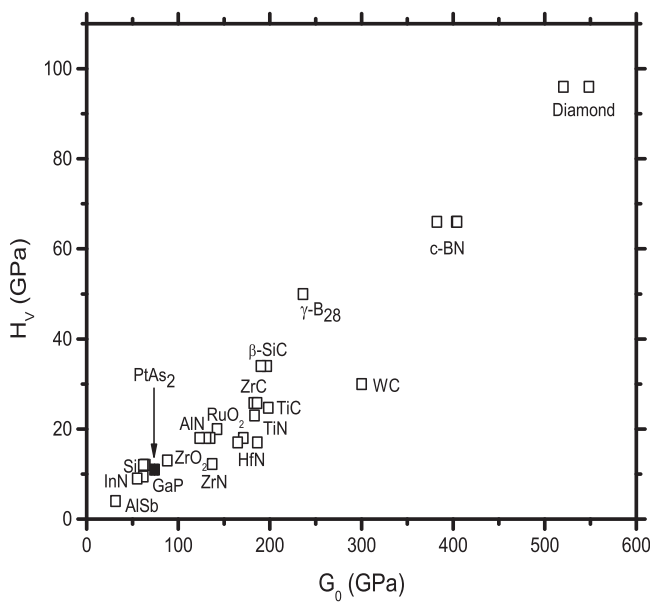

FIG. 3. Correlation of shear modulus G_0 and Vickers hardness H_V. Open squares: Data from Ref. 41, solid square: present result for $PtAs_2$.

TABLE II. Observed and calculated structure and elastic moduli of $PtAs_2$.

	Experiment	Theory GGA	Theory LDA
V_0 (Å^3)	212.46(5)	223.217	211.307
a_0 (Å)	5.9670(5)	6.066	5.956
x (-)	0.383(1)	0.38319	0.38305
Pt-As (Å)	2.489(2)	2.531	2.485
As-As (Å)	2.418(5)	2.455	2.413
H_V (GPa)	11.1(1)	9.9[a]	10.9[a]
		12.1[b]	12.3[b]
C_{11} (GPa)		290.3	339.1
C_{12} (GPa)		58.9	76.0
C_{44} (GPa)		67.4	76.6
K_0 (GPa)	220(5)	210(6)[c]	177(5)[c]
G_0 (GPa)	70(7)	83.8	95.3

[a]Based on the model given in Ref. 37.
[b]Based on the model given in Ref. 38.
[c]Based on a fixed pressure derivative of the bulk modulus of 1.5.

state determination was computed by relaxing the As internal coordinates at fixed volumes which is sufficient for cubic unit cells. The elastic constants at equilibrium were determined by applying two strains (strain 1: ε_{11} non-zero, and strain 2: ε_{44} non-zero, all other $\varepsilon_{ij} = 0$) of magnitude ± 0.01 to the equilibrium structure. The crystallographic coordinates were re-optimized for fixed strained unit cell and the elastic constants were determined from the resulting stress response to the applied strains by using Hooks law following previous studies.[37,38]

Bader charges were computed on a Γ-centered $16 \times 16 \times 16$ k-point grid relative to the sum of core and valance charge density.[39] The Bader charge analysis of the GGA equilibrium structure gives a charge transfer of 0.44e (GGA) and 0.49e (LDA) from As to Pt consistent with the higher (Pauling) electronegativity of Pt (2.28) as compared to As (2.18). Thus, the covalent overlap between Pt5d and As4p orbitals along with the above mentioned sterical constraints on the compression mechanism causes the observed low bulk compressibility. Calculated and observed internal structural coordinates at ambient pressure and at 35 GPa are equal, while the calculated bulk modulus is lower than observed (Table II). This suggests that the effective electron-electron repulsion between the non-bonding d-like states along the cubic axes and the As $pp\pi^*$ states and/or the electron density of these states is underestimated in the calculations. Hardness of $PtAs_2$ was estimated based on Simunek[40] and Chen *et al.*[41] models and match the experimentally observed hardness to within ±20% (Table II).

In conclusion, we find that $PtAs_2$ is exceptionally hard and incompressible among the known arsenides with a $K_0 = 220 \pm 5$ GPa, and $G_0 = 70 \pm 7$ GPa, and a mechanical micro-Vickers hardness of 11 ± 1 GPa. Thus, $PtAs_2$ compares with hard mononitrides such as ZrN and NbC, which is quite unusual for an arsenide. These mechanical properties in combination with its low indirect band gap of ~0.5 eV,[2,3] and chemical inertness make $PtAs_2$ interesting as material in electronic components. For instance, in contacts Pt-$PtAs_2$-GaAs or -AlAs formation of dislocations is expected in the substrate because the shear modulus of PtAs2 is much higher than that of GaAs and AlAs. In addition, the critical film thickness will decrease. It can be expected that the Schottky barrier height increases in the presence of $PtAs_2$ at the film-substrate interface. Generally, the low band gap in combination with its high hardness and chemical inertness may make $PtAs_2$ interesting for applications designed for tough environments. However, the rather low fracture toughness of $PtAs_2$ of 1.1–1.6 MPa $m^{1/2}$ may pose limits applications involving high torsional stress. With respect to the occurrence of $PtAs_2$ as interfacial component in Pt- and GaAs- or AlAs-based transistors[4,5] its brittleness and the large difference in elastic properties between these materials may cause fracturing upon lasting exposure to vibrations.

This research was supported by NNSA through DOE Cooperative Agreement DE-NA0001982. The Advanced Light Source is supported by the Director, Office of Science, Office of Basic Energy Sciences, of the U.S. Department of Energy under Contract No. DE-AC02-05CH11231.

[1]M. Sondergaard, M. Christensen, L. Bjerg, K. A. Borup, P. J. Sun, F. Steglich, and B. B. Iversen, Dalton Trans. **41**, 1278–1283 (2012).
[2]W. D. Johnston, R. C. Miller, and D. H. Damon, J. Less-Common Met. **8**, 272–287 (1965).
[3]J. H. Fermor, S. Furuseth, and A. Kjekshus, J. Less-Common Met. **11**, 376–377 (1966).
[4]A. Fricke, G. Stareev, T. Kummetz, D. Sowada, J. Mahnss, W. Kowalsky, and K. J. Ebeling, Appl. Phys. Lett. **65**, 755–757 (1994).
[5]H. Okada, S. Shikata, and H. Hayashi, Jpn. J. Appl. Phys., Part 2 **30**, L558–L560 (1991).
[6]W. Chen, J. S. Tse, and J. Z. Jiang, Solid State Commun. **150**, 181–186 (2010).
[7]J. C. Crowhurst, A. F. Goncharov, B. Sadigh, C. L. Evans, P. G. Morrall, J. L. Ferreira, and A. J. Nelson, Science **311**, 1275–1278 (2006).
[8]E. Gregoryanz, C. Sanloup, M. Somayazulu, J. Badro, G. Fiquet, H. K. Mao, and R. J. Hemley, Nature Mater. **3**, 294–297 (2004).
[9]P. F. McMillan, O. Shebanova, D. Daisenberger, R. Q. Cabrera, E. Bailey, A. Hector, V. Lees, D. Machon, A. Sella, and M. Wilson, Phase Transitions **80**, 1003–1032 (2007).
[10]M. Wessel and R. Dronskowski, J. Am. Chem. Soc. **132**, 2421–2429 (2010).
[11]S. Furuseth, K. Selte, and A. Kjekshus, Acta Chem. Scand. **19**, 735 (1965).
[12]A. Dewaele, P. Loubeyre, and M. Mezouar, Phys. Rev. B **70**, 094112 (2004).
[13]P. Dera, K. Zhuravlev, V. Prakapenka, M. L. Rivers, G. J. Finkelstein, B. Lavina, O. Grubor-Urosevic, O. Tschauner, S. M. Clark, and R. T. Downs, High Press. Res. **34**, 1–19 (2013).
[14]G. Sheldrick, Acta Crystallogr. **64**, 112–122 (2008).
[15]A. Zerr, M. Kempf, M. Schwarz, E. Kroke, M. Göken, and R. Riedel, J. Am. Ceram. Soc. **85**, 86–90 (2002).
[16]W. B. Holzapfel, High Press. Res. **22**, 209–216 (2002).
[17]X. Wu, G. Steinle-Neumann, S. Qin, M. Kanzaki, and L. Dubrovinsky, J. Phys.: Condens. Matter **21**, 185403 (2009).
[18]I. Shirotani, K. Yamanashi, J. Hayashi, N. Ishimatsu, O. Shimomura, and T. Kikegawa, Solid State Commun. **127**, 573–576 (2003).
[19]J. Z. Wu, H. Y. Zhu, D. B. Hou, C. G. Ji, C. E. Whiteley, J. H. Edgar, and Y. Z. Ma, J. Phys. Chem. Solids **72**, 144–146 (2011).
[20]S. Merkel, A. P. Jephcoat, J. Shu, H. K. Mao, P. Gillet, and R. J. Hemley, Phys. Chem. Miner. **29**, 1–9 (2002).
[21]T. Fujii, K. Tanaka, F. Marumo, and Y. Noda, Mineral. J. **13**, 448–454 (1987).
[22]P. Raybaud, J. Hafner, G. Kresse, and H. Toulhoat, J. Phys.: Condens. Matter **9**, 11107–11140 (1997).
[23]D. Nguyen-Manh, P. S. Ntoahae, D. G. Pettifor, and P. E. Ngoepe, Mol. Simul. **22**, 23–30 (1999).
[24]N. Cuadrado, D. Casellas, M. Anglada, and E. Jimenez-Pique, Scr. Mater. **66**, 670–673 (2012).
[25]B. R. Lawn, A. G. Evans, and D. B. Marshall, J. Am. Ceram. Soc. **63**, 574–581 (1980).
[26]M. T. Laugier, J. Mater. Sci. Lett. **6**, 897 (1987).
[27]D. K. Shetty, I. G. Wright, P. N. Mincer, and A. H. Clauer, J. Mater. Sci. **20**, 1873–1882 (1985).

[28]R. W. Hertzberg, *Deformation and Fracture Mechanisms of Engineering Materials*, 3rd ed. (Wiley, New York, 1989).
[29]A. Kelly and N. H. Macmillan, *Strong Solids*, 3rd ed. (Clarendon Press, Oxford, 1986).
[30]D. M. Teter, MRS Bull. **23**, 22–27 (1998).
[31]G. Kresse and J. Furthmuller, Phys. Rev. B **54**, 11169–11186 (1996).
[32]G. Kresse and J. Hafner, Phys. Rev. B **48**, 13115–13118 (1993).
[33]J. P. Perdew and A. Zunger, Phys. Rev. B **23**, 5048–5079 (1981).
[34]J. P. Perdew, K. Burke, and M. Ernzerhof, Phys. Rev. Lett. **77**, 3865–3868 (1996).
[35]P. E. Blochl, Phys. Rev. B **50**, 17953–17979 (1994).
[36]G. Kresse and D. Joubert, Phys. Rev. B **59**, 1758–1775 (1999).
[37]B. B. Karki, L. Stixrude, and R. M. Wentzcovitch, Rev. Geophys. **39**, 507–534, doi:10.1029/2000RG000088 (2001).
[38]B. Kiefer, S. R. Shieh, T. S. Duffy, and T. Sekine, Phys. Rev. B **72**, 014102 (2005).
[39]W. Tang, E. Sanville, and G. Henkelman, J. Phys.: Condens. Matter **21**, 084204 (2009).
[40]A. Simunek, Phys. Rev. B **80**, 060103 (2009).
[41]X. Q. Chen, H. Y. Niu, D. Z. Li, and Y. Y. Li, Intermetallics **19**, 1275–1281 (2011).